HHS Public Access

Author manuscript

Cancer Immunol Res. Author manuscript; available in PMC 2018 March 01.

Published in final edited form as:

Cancer Immunol Res. 2017 March ; 5(3): 198–210. doi:10.1158/2326-6066.CIR-16-0304.

Differentiated state of initiating tumor cells is key to distinctive immune responses seen in H-Ras^{G12V}–induced squamous tumors

Michael A. Podolsky[1], **Jacob T. Bailey**[1], **Andrew J. Gunderson**[2], **Carrie J. Oakes**[1], **Kyle Breech**[1], and **Adam B. Glick**[1]

[1]The Pennsylvania State University, The Huck Institutes of the Life Sciences, State College, PA

[2]Earle A. Chiles Research Institute, Portland, OR

Abstract

Heterogeneity in tumor immune responses is a poorly understood yet critical parameter for successful immunotherapy. In two doxycycline-inducible models where oncogenic H-Ras^{G12V} is targeted either to the epidermal basal/stem cell layer with a Keratin14-rtTA transgene (K14Ras), or committed progenitor/suprabasal cells with an Involucrin-tTA transgene (InvRas) we observed strikingly distinct tumor immune responses. On threshold doxycycline levels yielding similar Ras expression, tumor latency, and numbers, tumors from K14Ras mice had an immunosuppressed microenvironment while InvRas tumors had a pro-inflammatory microenvironment. On a *Rag1*$^{-/-}$ background InvRas mice developed fewer and smaller tumors that regressed over time while K14Ras mice developed more tumors with shorter latency than *Rag1*$^{+/+}$ controls. Adoptive transfer and depletion studies revealed that B and CD4 T cell cooperation was critical for tumor yield, lymphocyte polarization, and tumor immune phenotype in *Rag1*$^{+/+}$ mice of both models. Coculture of tumor-conditioned B cells with CD4 T cells implicated direct contact for Th1 and regulatory T cell (Treg) polarization, and CD40-CD40L for Th1, Th2, and Treg generation, a response not observed from splenic B cells. Anti-CD40L caused regression of InvRas tumors but enhanced growth in K14Ras, while a CD40 agonist mAb had opposite effects in each tumor model. These data show that position of tumor initiating cells within a stratified squamous epithelial tissue provokes distinct B and CD4 T cell interactions, which establish unique tumor microenvironments that regulate tumor development and response to immunotherapy.

Keywords

Ras; CD40; B Cell; Skin carcinogenesis; Checkpoint therapy

Introduction

Heterogeneity in tumor immune responses are well documented but the underlying mechanisms generating distinct tumor immune phenotypes remain poorly understood. Many cancers develop an immunosuppressive microenvironment, dampening antitumor immunity

Corresponding Author: Adam B. Glick, 306C Life Sciences Building, Shortlidge Road, University Park, PA 16802, 814-865-7170, Abg11@psu.edu.

The authors declare no potential conflicts of interest.

and facilitating tumor growth (1–3), whereas in others, chronic inflammation creates microenvironments that increase the risk of cancer development and enhance tumor growth (4, 5). Molecular and immune phenotyping has revealed the heterogeneity of underlying genetic changes and signaling pathways, which is linked to different immune signatures, responses to therapy, and outcomes for individual patients with the same tumor types (6–9). Different immune microenvironments show heterogeneity at the cellular level: Regulatory T cells (Tregs) (10, 11), helper T cells (Th cells) (12), B cells (13, 14), and myeloid cells (15, 16) have been described with both tumor-suppressive and tumor-promoting properties. Between different tumors, this may reflect diverse interactions between multiple cell types within the tumor microenvironment, differences in tumor cell genetics and signaling, tumor type, or progression of tumors through immunoediting to escape (17). This presents challenges in developing immunotherapies, as patients may show improved or worsened prognosis depending upon relationships between the tumor and its immune microenvironment. Patients with melanoma (18), lung cancer (19), gastric cancer (20), renal cell carcinoma (21), and head and neck cancer (22, 23) have all benefited from advances in immune checkpoint blockade, but tumors perpetuated by chronic inflammation, such as colorectal carcinoma (CRC) (24), hepatocellular carcinoma (25), as well as hematological malignancies, benefit from reducing tumor-promoting inflammation (26).

It is not known to what extent the immune phenotype of a tumor is impacted by the initiating transformed cell. Most solid tumors arise from hierarchically organized epithelia comprised of tissue stem cells, transit amplifying cells, and differentiated cells (27, 28). Studies in murine models of cutaneous cancer in which c-H-Ras mutations drive tumor development show that carcinogen treatment or oncogene activation in different progenitor cell populations can give rise to distinct tumor phenotypes (29–31). We previously showed that benign epidermal squamous lesions with a high frequency for progression to squamous cell carcinoma (SCC) exhibit a gene expression pattern associated with reduced inflammation, relative to lesions with a low frequency for progression (32). To test if oncogene activation in different tumor-initiating cell populations impacts the tumor immune response, we generated mice with inducible expression of human H-Ras^{G12V} targeted to either basal/stem cells or committed progenitor/suprabasal cells of the epidermis (28). Here we show that within a single epithelium the same driver oncogene can generate opposite immune responses and response to immunotherapies, depending on the origin of the tumor initiating cell. These distinct immune responses of either immunosuppression or tumor-promoting inflammation are driven by B cell and CD4 T cell cooperation within the tumor microenvironment. These results offer insight into the intricacies of modulating the tumor immune microenvironment, and provide guidance for the application and scope of immunotherapeutics in cancer treatment.

Materials and Methods

Animal Studies

Tetracycline-regulated transactivators (tTA) driven by involucrin (Inv) [InvtTA (33)] (obtained from Dr. Julie Segre) or reverse tetracycline-regulated transactivators (rTA) driven by Keratin-14 (K14) [K14rTA (34)] mice (The Jackson Laboratory) were crossed with

homozygous tetOH-Ras^{G12V} (35) mice, (NCI Mouse Repository) producing double transgenic (DT) InvtTA/tetOH-Ras^{G12V} (InvRas) or K14rTA/tetOH-Ras^{G12V} (K14Ras) mice. Suppression of transgene expression in InvRas mice was accomplished with 10 μg/mL doxycycline hyclate (Sigma-Aldrich) administered *ad libitum* in drinking water. Tumors were induced in shaved 7 week old mice by reducing doxycycline to 250 ng/ml for InvRas mice and administration of 7.5 μg/mL doxycycline in drinking water to K14Ras mice. Tumors were counted and measured every 48–72 hours, and harvested 28–32 days following Ras induction, or if animals were moribund. To control for gender differences, when possible equal numbers of male and female mice were used, and all data represent results from both genders. Cell counts were conducted using a Cellometer Auto T4 Cell Viability Counter (Nexcelom Bioscience). All mice were on the FVB/n background.

To deplete leukocytes, mice were given 500 μg of GK1.5 (anti-CD4), 5D2 (anti-CD20), RB6-8C5 (anti–GR-1), isotype control HB94 or anti-ragweed IgG weekly intraperitoneally beginning 7 days prior to tumor induction, or every other day beginning one day prior to H-Ras^{G12V} induction (anti–GR-1). GK1.5, RB6-8C5 and HB94 hybridomas were obtained from ATCC, 5D2 and anti-IgG antibody were obtained from Genentech. Anti-CD40L (BioXCell) was injected 7 days prior to tumor induction, or upon tumor presentation, followed previously defined methods (36). CD40 agonist–treated mice were injected with 100 μg FGK4.5 (BioXCell) weekly beginning at indicated days. Anti-CD40L and CD40 agonist antibodies were tested to be free of endotoxin (< 0.002 EU/μg, BioXCell). *Rag1*$^{-/-}$ mice were reconstituted by retro-orbital administration of 5 million CD4 T cells or B cells from spleens of healthy age-matched syngenic mice (StemCell Easysep), or phosphate-buffered saline (PBS). Studies were performed in compliance with the U.S. Department of Health and Human Services Guide for the Care and Use of Laboratory Animals, and after approval by The Pennsylvania State University Institutional Animal Care and Use Committee.

Flow Cytometry

Skin leukocytes were isolated as previously described (37), incubated with antibodies in 1% BSA/PBS at 1 × 10^7 cells/mL. Leukocytes were stimulated for intracellular cytokines in complete RPMI 1640 medium (38). Following 4% paraformaldehyde fixation, cells were permeabilized and stained using 0.2% Saponin/1% BSA/1x PBS at 1 × 10^7 cells/mL. Cells were analyzed using an LSRFortessa Cytometer (BD Biosciences) and FlowJo version 7. Myeloid cells were gated on Live CD45$^+$, CD11b$^+$, followed by Ly6G$^+$/Ly6C$^+$ for neutrophils, Ly6G$^-$/Ly6C$^+$ for MDSC, and Ly6G$^-$/Ly6C$^-$/F4/80$^+$ for macrophages. CD4 T cells were gated on Live CD45$^+$, CD3$^+$, CD4$^+$, followed by IFNγ (Th1), IL-4 (Th2), IL-17 (Th17), or FoxP3 (Treg). B cells were gated on Live CD45$^+$, CD19$^+$, CD45R$^+$, MHCII+ followed by CD1d^{hi}/CD5$^+$ (Breg), and CD40$^+$/CD80$^+$/CD86$^+$ (APC+). Live cells were identified using LIVE/DEAD® Fixable Yellow Dead Cell Stain Kit (Life Technologies).

Protein and RNA Analysis

Protein and RNA was isolated from tumors and analyzed by immunoblotting and RT-qPCR respectively, as described (39), using β-actin as loading control.

Histological Analysis

Formalin fixed sections were stained with hematoxylin and eosin using a ST5010 Autostainer XL (Leica Biosystems). For anti-CD45 and anti-Ki67 immunohistochemistry, formalin fixed sections were pretreated with Tris-based antigen unmasking solution (Vector labs) according to manufacturer's protocol. Antibodies were detected using VECTASTAIN® ImmPRESS (Vector Laboratories). Anti-keratin immunohistochemistry was done on ethanol-fixed sections with ImmPACT DAB (Vector Laboratories) detection system. For co-immunofluorescence, 7 μm frozen sections were incubated with anti-CD4 (1:100, Biolegend) followed by IgG-Alexa Fluor® 647 (1:500, Biolegend), biotinylated anti-CD19 (1:100, Biolegend), streptavidin-Alexa Fluor® 488 (1:500, Biolegend) using the Polink Double Staining System (GBI Labs). VECTASHIELD Mounting Medium with DAPI (Vector Laboratories) was used to visualize nuclei.

Lymphocyte Coculture

CD4 T cells and B cells were purified from spleen or tumor tissue and plated onto 24-well plates coated with mAbs to CD3 and CD28 (Biolegend). Lymphocytes were suspended in complete RPMI1640 media and CD4 T cells were added first followed by hamster IgG, anti-CD40L, or Transwell inserts (BD Falcon®), then B cells. Cells were incubated for 7 days at 37°C and 5%CO_2 with fresh media added every 48 hours and stained for flow cytometry as indicated.

Suppression Assays

Negatively selected purified B cells from tumor tissue and CD4 T cells from spleens were cocultured seven days following staining with 2.5μM CFSE. Harvested cells were analyzed by flow cytometry for CFSE dilution. For MDSC suppression assays, mice were placed on doxycycline chow for 4 days (Bio-Serv) (K14Ras), or 7 days doxycycline removal (InvRas), splenocytes were stained with αCD11b, αLy6G, and αLy6C, and then sorted using a Cytopeia Influx Sorter (BD Biosciences). Sorted cells were incubated with stimulated naïve CD8 T cells for 72 hours and analyzed by flow cytometry for CFSE dilution.

Statistical Analysis

For experiments with only two groups of study, Student's *t* tests were used. If three or more groups were compared, one-way ANOVA was used with Newman-Keuls post-analysis. All figures, graphs, and statistical analyses were made using GraphPad Prism 4.0. *, $P < 0.05$; **, $P < 0.01$; ***, $P < 0.001$.

Results

Distinct immune phenotypes generated by H-Ras^{G12V} expression in different epidermal cell populations

Papillomas at high risk or low risk for progression to SCC have distinct immune signatures (32). Because these tumors may arise from different initiating cells, we examined whether targeting oncogenic Ras to different cellular compartments of the murine epidermis, using inducible models of squamous tumorigenesis, altered tumor-associated immune responses.

These models allow for specific targeting of the activated H-Ras^{G12V} oncogene to either the basal/stem cell (K14Ras) or committed progenitor/suprabasal epidermal compartments (28). When 7-week-old InvRas and K14Ras bitransgenic mice were placed on threshold doses of doxycycline, focal tumors arose in both groups with similar kinetics (first appearance 7–10 days) and numbers (Fig. 1A), and expression of H-Ras and ERK1/2 (phosphorylated and total) (Supplementary Fig. S1A), although by 24 days the average volume of K14Ras tumors was greater than InvRas tumors (Fig. 1B). Immunohistochemical staining with hematoxylin and eosin (H&E) and anti-keratin showed that basal expression of H-Ras^{G12V} generated SCC), whereas suprabasal expression induced squamous papillomas (Supplementary Fig. S1B), similar to previous studies (29). Despite similar expression, targeting H-Ras^{G12V} to different cell populations within the epidermis caused distinct tumor immune responses. Expression of Th1- (TNFα), Th2- (IL33, thymic stromal lymphoprotein (TSLP), and lymphotoxin (LT)), and Th17- (IL6, TGFβ) associated genes was significantly higher in InvRas than K14Ras tumors. Although not statistically significant, IL12 was also more highly expressed in InvRas. In addition to the overall reduced level of pro-inflammatory cytokines, K14Ras tumors expressed more immunosuppressive cytokine IL10, although no differences were observed for IL35 (Fig. 1C–F).

Consistent with these cytokine signatures, InvRas tumors had significantly higher percentages of Th2 cells and more pro-inflammatory antigen-presenting B cells (APC+), whereas K14Ras tumors had significantly higher percentages and numbers of Tregs and Bregs (Fig. 1G–J). Tumor-infiltrating B cells from K14Ras, but not InvRas, tumors caused significant suppression of CD4 proliferation in coculture (Fig. 1K), confirming their specific regulatory capacity. No significant differences in cell numbers or percentages were observed in splenic T or B cells (Supplementary Fig. S1C and D). CD45 immunohistochemistry showed significantly more leukocytes infiltrating into InvRas tumors compared to K14Ras (Supplementary Fig. S2).

To rule out that differences observed in immune phenotype were indirectly the result of distinct tumor phenotypes, we induced strong expression of Ras in both models and examined the response after 5 days. High Ras expression caused neutrophil microabscesses in InvRas mice but not K14Ras (Supplementary Fig. S3A). Additionally, patterns of cytokine expression (Supplementary Fig. S3B) were distinct and circulating CD11b^{+} Ly6G^{-} cells that could suppress CD8 T cell proliferation *in vitro* were significantly expanded in K14Ras but not InvRas mice, in agreement with increased arginase1 expression in hyperplastic K14Ras skin (Supplementary Fig. S3C–E). Together these results show that responses to oncogenic Ras are distinct at the earliest time points, even under conditions of supraphysiological Ras expression.

Lymphocytes promote or suppress tumor development dependent on tumor-initiating cell

To determine the specific effects of lymphocytes on Ras-driven tumor development, both models were crossed onto a *Rag1*$^{-/-}$ background and tumors induced as described above. K14Ras*Rag1*$^{-/-}$ mice developed a significantly greater number of tumors that grew faster than *Rag1*$^{+/+}$ counterparts, with few mice surviving beyond 14 days (Fig. 2A–C). In contrast, tumors in InvRas*Rag1*$^{-/-}$ mice began to regress 15 days after Ras induction; by 18

days *Rag1*$^{+/+}$ mice had significantly more tumors, despite an initially similar tumor incidence. Additionally, tumors developing in InvRas*Rag1*$^{-/-}$ mice were smaller on average than tumors from their *Rag1*$^{+/+}$ counterparts, but variability in tumor size prevented statistical significance (Fig. 2D–F). The percentages of tumor-infiltrating neutrophils in K14Ras mice increased in the absence of lymphocytes (Fig. 2G,H), but there was a striking reduction in neutrophils in InvRas*Rag1*$^{-/-}$ mice, leading to a change in proportion of myeloid cell populations within the tumor (Fig. 2I,J). Additionally, CD45 staining confirmed reduced leukocyte infiltration into tumors of InvRas*Rag1*$^{-/-}$ mice, but increased in K14Ras*Rag1*$^{-/-}$ mice, and leukocytes infiltrated the tumor parenchyma in all models (Supplementary Fig. S2). When H-Ras^{G12V} was strongly induced in the epidermis of mice depleted of neutrophils with anti–GR-1, proliferation of basal cells was significantly reduced compared to isotype control (Supplementary Fig. S2), suggesting that tumor-infiltrating neutrophils could enhance tumor growth. Together these results suggested that immunoregulation in basal/stem cell Ras-driven tumors was associated with a decreased tumor burden whereas greater inflammation in committed progenitor/suprabasal-Ras driven tumors led to enhanced tumor burden.

Tumor-initiating cell drives distinct CD4 T cell – B cell interactions that determine immune response

The absence of lymphocytes generated opposite responses between the tumor models. We therefore determined which lymphocyte subsets drove the distinct tumor responses, using adoptive transfer of CD4, CD8, and B cells alone or in combination into *Rag1*$^{-/-}$ mice. Although adoptive transfer of naïve CD4 T cells or B cells alone had no significant effect on tumor numbers in K14Ras*Rag1*$^{-/-}$ mice, co-transfer of CD4 T cells with B cells reduced tumor numbers to *Rag1*$^{+/+}$ levels, although suppressive effects were lost after 20 days (Fig. 3A). Adoptive transfer of CD4 T cells or B cells into InvRas*Rag1*$^{-/-}$ mice suppressed tumor development, whereas co-transfer restored a tumor-promoting phenotype similar to *Rag1*$^{+/+}$ mice until day 20 (Fig. 3B). Adoptive transfer of CD8 T cells or co-transfer of CD8 with B cells reduced tumor numbers in K14Ras and InvRas*Rag1*$^{-/-}$ mice, but this was not statistically significant compared to *Rag1*$^{-/-}$. Although co-transferred K14Ras mice had fewer tumors, epidermal hyperplasia was more pronounced and mice became moribund more quickly, suggesting that this was not a protective immune response. CD8 T cells caused an overall suppression of both Bregs and APC+ subsets, inconsistent with phenotypes observed in *Rag1*$^{+/+}$ mice (Supplementary Fig. S4A–D), suggesting that CD8 T cells have little overall impact on determining the *Rag1*$^{+/+}$ immune responses in either model. Supporting the opposing functions of lymphocytes in these two tumor models, depletion of either CD4 T cells or B cells from K14Ras*Rag1*$^{+/+}$ mice resulted in a similar increase in tumor number, whereas depletion from InvRas*Rag1*$^{+/+}$ mice resulted in suppression of tumor formation (Fig. 3C and D). Together these data suggest that the nascent tumor microenvironment programs CD4 T and B cells towards distinct cooperating phenotypes that either suppress (K14Ras) or enhance (InvRas) tumor development.

To test this, we examined the phenotype of tumor infiltrating lymphocytes (TILs) in tumors from mice receiving CD4 T and B cells alone or together. TILs from CD4 T-cell transfers into K14Ras*Rag1*$^{-/-}$ mice were skewed towards a pro-inflammatory Th1 phenotype with

reduced Tregs, whereas co-transfer restored Th1 and Tregs to *Rag1*$^{+/+}$ levels (Fig. 3E). In contrast, TILs from CD4 T-cell transfers into InvRas*Rag1*$^{-/-}$ mice exhibited polarization towards Tregs, with slightly reduced percentages of Th1 cells. Importantly, co-transfer caused a minor increase in Th1 cells and a significant increase in Th17 cells, but reduced Tregs (Fig. 3F). Co-transfer of B and CD4 T cells selectively restored expression of CD4 associated genes to *Rag1*$^{+/+}$ levels of each model. Co-transfer into K14Ras*Rag1*$^{-/-}$ mice reduced expression of IL12, IL33, TSLP, and IL35 in tumors, whereas co-transfer into InvRas*Rag1*$^{-/-}$ mice completely restored IL33 and IL35 expression. IL12 expression was higher and TSLP expression was lower than *Rag1*$^{+/+}$ in co-transferred tumors but not statistically different from *Rag1*$^{+/+}$. IL1β expression was not significantly affected by co-transfer (Supplementary Fig. S5A–E). Co-transfer also regulated the phenotype of B-cell TILs (TILBs) in opposite directions: B cells transferred into K14Ras*Rag1*$^{-/-}$ mice had increased APC+ percentages, whereas co-transfer restored APC+ B cells to that of *Rag1*$^{+/+}$ tumors (Fig. 3G). In contrast, co-transfer into InvRas*Rag1*$^{-/-}$ mice decreased the percentage of Bregs compared to B-cell transfer, although APC+ B cells were not affected (Fig. 3H). These altered lymphocyte phenotypes had pronounced effects on tumor-infiltrating neutrophils. Only co-transfer of CD4 T and B cells could reduce neutrophil percentages to that of *Rag1*$^{+/+}$ levels in K14Ras*Rag1*$^{-/-}$, and recover neutrophils in InvRas*Rag1*$^{-/-}$ (Fig. 3I and J), likely the result of the recovery and suppression of Tregs, respectively. The percentage of dendritic cell (DC) subsets within the skin draining lymph nodes or skin differed little between K14Ras and InvRas mice, except for plasmacytoid DC and CD11b^{-} DC, but these were not closely correlated with the overall immunophenotype, as InvRas tumors had fewer pro-inflammatory plasmacytoid dendritic cells and K14Ras tumors had fewer immunoregulatory CD11b^{-} lymphoid dendritic cells (Supplementary Fig. S6A–J), indicating that the polarizing effect could not be carried out by dendritic cells alone, and that B cell presence was necessary for proper CD4 T cell polarization. These results indicate that CD4 T cells and B cells cooperated to produce an immunosuppressive microenvironment in K14Ras mice that constrained tumor outgrowth, whereas cooperation in InvRas mice resulted in a pro-inflammatory microenvironment supporting tumor growth.

Divergent polarization of CD4 T cells required direct contact and CD40/CD40L interaction

Transferred B cells in both models were largely present within tumors, but not in secondary lymphoid nodes (Supplementary Fig. S7), which prompted us to hypothesize that B cells largely affect CD4 T-cell polarization within the tumor microenvironment. To test the effects of tumor-conditioned B cells on CD4 polarization, we cocultured TILB or splenic B cells from tumor bearing mice or healthy controls with anti-CD3/CD28–stimulated naïve CD4 T cells from nontransgenic mice. K14Ras TILBs polarized naïve CD4 T cells towards Treg and away from Th2, whereas InvRas TILB facilitated Th2, but not Treg, polarization. Splenic B cells from tumor-bearing mice had a distinct phenotype, suppressing both Treg and Th1 polarization relative to stimulated controls, but this was not different from B cells of nontransgenic mice. These results suggested that the specific polarization of CD4 T cells by B cells required conditioning by the tumor microenvironment (Fig. 4A–D). Co-immunofluorescence showed these cells in direct contact within the tumor parenchyma of both models, indicating a potential mechanism for interaction within the tumor microenvironment (Fig. 4E,F). We did not observe any tertiary lymphoid structures within

tumors of either model, as others have previously reported (13, 40, 41), although this may be due to differences in model systems or time-course.

To determine if direct contact was needed for polarization, stimulated naïve CD4 T cells were separated from tumor-conditioned B cells of either K14Ras or InvRas mice using transwell inserts. K14Ras tumor-conditioned B cells significantly increased the overall percentage of Tregs, but did not affect pro-inflammatory subsets. Additionally, when direct contact was blocked, the percentage of Th1 cells increased and Tregs significantly decreased. These data suggest that direct contact from K14Ras TILBs could polarize naïve CD4 T cells towards a Treg phenotype and away from Th1 (Fig. 5A–D). In contrast, blocking contact from InvRas TILB caused a decrease in Th1 and Th17 cells, and a significant increase in Tregs (Fig. 5A–D). Preventing direct contact had no effect on the ability of InvRas TILB to polarize Th2 cells.

The CD40/CD40L pathway is critical for the establishment of humoral responses as perpetuated by Th2/B cell interactions, is implicated in immune responses to several cancers, and is a potential target for immune checkpoint blockade (42). To test if CD40/CD40L interactions were important for TILB effects on CD4 polarization, a CD40L blocking antibody (MR-1, BioXcell) was included in coculture assays. Blockade of CD40/CD40L between K14Ras TILBs and naïve stimulated CD4 T cells caused a significant increase in percentage of Th1 and Th2 cells and simultaneously decreased the percentage of Tregs, with little effect on Th17 (Fig. 5E–H). In contrast, blockade of CD40/CD40L from InvRas TILBs caused a marked increase in Treg differentiation and a slight, but not statistically significant, reduction in all pro-inflammatory CD4 subsets (Fig. 5E–H). Thus, the effects on CD4 polarization caused by blockade of direct cell-cell contact with transwell inserts was likely due to inhibition of CD40/CD40L interactions between TILBs and CD4 T cells. We conclude that CD40/CD40L interactions were the primary mechanism by which CD4 T cells and B cells interacted within the tumor microenvironment to orchestrate the Th1/Treg balance, and that Th2 polarization by InvRas TILB was a direct result of CD40 ligation.

Tumor initiating cell governs *in vivo* responses to therapeutic antibodies targeting CD40/CD40L

Given the distinct tumor immune responses generated by targeting H-Ras^{G12V} to different epidermal cell populations, and divergent effects of CD40/CD40L blockade on TILB polarization of CD4 T cells, we examined how *in vivo* blockade of CD40/CD40L would affect tumor development. In a pretreatment protocol, mice were given anti-CD40L seven days prior to H-Ras^{G12V} induction, and were given weekly boosters as described (35). In anti-CD40L–treated K14Ras mice, tumor numbers were slightly elevated compared to isotype control injected mice (Fig. 6A). In contrast, anti-CD40L pretreatment significantly reduced the number of tumors that developed in InvRas mice (Fig. 6B). To determine the effect of CD40 blockade in a therapeutic setting, mice were injected with anti-CD40L or isotype control antibody after tumors became palpable on either day 14 or day 11 for K14Ras and InvRas mice respectively. Under these conditions, tumor numbers were not significantly affected over time in either tumor model (Fig. 6C,D). Anti-CD40L treatment

significantly altered tumor growth in opposite directions. In K14Ras mice, anti-CD40L caused a 10-fold greater increase in tumor volume relative to initial tumor volume compared to isotype control injected mice (200-fold increase versus 20-fold increase) (Fig. 6E). In contrast, anti-CD40L injection in tumor bearing InvRas mice prevented further tumor growth or caused regression after an initial period of growth. Continuous tumor growth (70-fold over starting volume on day 22) was only observed in isotype control injected mice (Fig. 6F). The decrease in fold change in InvRas isotype control mice from day 22 to day 24 occurred due to sacrifice of moribund mice at day 22 for humane endpoints.

CD40 agonist antibodies are in clinical trials as therapeutic antibodies (43). To determine if opposite tumor responses would also occur when CD40 was activated, K14Ras or InvRas mice were injected with FGK4.5, a CD40 agonist mAb, after tumors had developed. CD40 agonist mAb significantly reduced the number of tumors in K14Ras mice, but had no effect on tumor number in InvRas (Fig. 6G,H). Furthermore, and in contrast to treatment with anti-CD40L, tumors in CD40 agonist treated K14Ras mice grew much more slowly compared to isotype control with only a 10-fold increase in volume compared to 60-fold for isotype control relative to starting volume (Fig. 6I). In contrast, tumors from InvRas mice treated with CD40 agonist had on average a 190-fold increase in tumor volume relative to starting volume, as compared to 50-fold increases in isotype controls at study end (Fig. 6J). Together these data show that the specific tumor immune microenvironment could alter the direction of response to therapeutic antibodies.

Discussion

Here we show that oncogenic $HRas^{G12V}$ expression within cell types with distinct fates in the differentiation hierarchy of the epidermis generated highly divergent immune responses that promoted or suppressed tumor development. When expressed in the basal/stem cell or committed progenitor/suprabasal compartments, oncogenic Ras caused either an immunosuppressive Treg dominated, or pro-inflammatory Th2 dominated, microenvironment; B cell–driven Treg or Th1/2 polarization via CD40/CD40L ligation; and anti-CD40L–mediated promotion or suppression of tumor development. Although the models utilize an inducible system and therefore likely have higher expression of Ras than mutations of the endogenous locus, we have titered doxycycline to threshold doses that give focal tumor development and similar expression of oncogenic Ras and activation of downstream signaling. The mechanism by which these distinct immune responses are generated is not clear. Given the distinct location and properties of dendritic cell subsets in the skin, differential activation of one or more subsets in response to Ras expression in keratinocytes is a possibility, although we did not observe differences between the tumor models in DC subsets in the skin draining lymph nodes shortly after induction of Ras. Differential activation or polarization of skin resident γδ T cells, previously shown to play an important role in squamous tumor development (44), could also be important. Keratinocytes themselves are known to produce inflammatory mediators such as CD40 (45), TNFα, and multiple interleukins that can mediate both pro and antitumor inflammation (46). Although the ERK1/2 MAPK pathway was activated similarly in both models, it is possible that other Ras effector pathways are differentially engaged in keratinocytes, leading to divergent expression of immunoregulatory genes and pathways. That distinct cytokine

expression and immune responses occurred rapidly in the epidermis following induction of strong Ras expression supports the idea that the distinct tumor immune phenotypes observed reflects distinct properties of the tumor-initiating cell rather than a consequence of tumor stage or histology. Nevertheless, these results, together with our previous study showing that chemically induced tumors with a high-risk and low-risk for progression to SCC had distinct immune signatures (32), suggest that heterogeneity in human cancer immune phenotypes within single tissues could reflect the location of the cancer-initiating cell or cancer stem cell within the stem cell hierarchy of the tissue.

As no lymphocyte was able to restore a $Rag1^{+/+}$ tumor phenotype when transferred to K14Ras or InvRas $Rag1^{-/-}$ mice, we co-transferred either CD4 or CD8 T cells with B cells into $Rag1^{-/-}$ mice of each model. In K14Ras mice, CD8 plus B cell co-transfer caused fewer tumors, due to a generalized epidermal hyperplasia but with rapid mortality, whereas in InvRas mice co-transfer was unable to restore tumor development. CD4 T and B cell co-transfers restored $Rag1^{+/+}$ tumor numbers in both models, without a generalized epidermal hyperplasia, suggesting that the interactions between these two subsets were critical for the observed immunosuppressive and tumor promoting immune responses. Both CD4 T cells and B cells have been extensively studied in a number of human cancers and mouse models, with each having distinct pro and antitumor functions. Tregs have a controversial role in SCC. They inhibit antitumor responses through CTLA-4, CD25, CD39, CD73, IL10, and TGFβ in a tumor antigen–specific manner (47), and also increase growth and metastasis directly through RANK signaling (48). On the other hand, Tregs are associated with improved prognosis in SCC, as higher Treg counts in early stage oral SCC are associated with improved survival and decreased lymph node metastasis (47). Bregs display fewer surface CD20 molecules, causing anti-CD20 administration to enrich for Bregs within the total B cell repertoire (49). Although Tregs and Bregs are most commonly associated with tumor escape (13), we find that the predominant Treg and Breg immunosuppressive phenotype found in the K14Ras tumors was associated with suppression of tumor outgrowth, in agreement with previous reports in both mouse and human SCC (50–52). The likely mechanism for this tumor suppression is through inhibition of neutrophils that enhance proliferation of transformed keratinocytes, as CD4 T and B cell co-transfer significantly reduced percentages of tumor-infiltrating neutrophils. Tregs improve clinical outcome in many hematological cancers including follicular lymphoma, diffuse large B cell lymphoma, and Hodgkin lymphoma (53). Additionally, Th2 cells are also associated with tumor escape in pancreatic, mammary, and colitis-associated cancers, specifically attributed to IL13 (54), IL4- and IL10-inducing M2 macrophages (55), and TGFβ and IL5 (56), respectively. We find that Th2 cells predominate in a pro-inflammatory setting that promotes tumor formation.

Although the cross-polarizing roles of CD4 T cells and B cells has been previously reported (13), we have now directly compared these interactions in a stratified squamous epithelium, comparing tumors of stem and differentiated cell origins. We show that direct interaction and cross polarization between CD4 T and B cells through CD40/CD40L is essential for establishment of both tumor immune phenotypes. Adoptive transfer studies showed that both lymphocytes were needed to reproduce the tumor immune phenotype of $Rag1^{+/+}$ mice. These results also suggest that APC function of innate leukocytes such as dendritic cells is

not sufficient to polarize CD4 T cells or B cells towards the immune phenotype seen in *Rag1*$^{+/+}$ mice. Specific depletion of these lymphocytes enhanced tumor numbers in K14Ras and suppressed in InvRas mice. However, although CD4 T cells could be fully depleted, anti-CD20 depletion enriched for Bregs, as shown by others (49) (data not shown), suggesting that simple disruption of the CD4 and B cell dynamic results in perturbation of the *Rag1*$^{+/+}$ tumor response.

Co-transferred B cells were found only in tumor tissue and not inguinal lymph nodes, indicating a localized immune response (Supplementary Fig. S7). In many models, including mouse and human SCC, tertiary lymphoid structures are found within the tumor microenvironment, acting as a surrogate localized lymph node (13, 40, 41). We did not observe lymphoid structures within tumor tissue of either mouse model, and lymphocytes appeared to be localized within the tumor parenchyma. Supporting the idea that the critical interaction between B and T cells occurred within the tumor, we found that only B cells from tumor tissue, but not splenic B cells of tumor-bearing mice, could specifically polarize CD4 T cells in coculture towards the *Rag1*$^{+/+}$ phenotype. The specific tumor microenvironment was critical for determining the ability and direction of naïve CD4 polarization by TILBs. Although direct contact in coculture was essential for TILB polarization of Tregs and Th1 cells, prevention of contact had no effect on Th2 percentages, compared to coculture controls. Blockade of CD40L showed similar results as transwell inserts, but also inhibited B cell effects on Th2 polarization. Activated B cells can secrete soluble CD40 (57), thus although direct cell contact is necessary for polarizing signals of Th1 and Tregs, it is possible that Th2 polarization is influenced by B cell–derived CD40. B cells can both promote or suppress tumor formation by acting as plasma cells, APCs, or Bregs, secreting TGFβ, IL10, IL4, and other interleukins to modulate pro and anti-inflammatory CD4 and CD8 T cells (13). Specific downstream mechanisms beyond CD40/CD40L were not determined in these studies, however alternative local cytokine expression by B cells are the most likely mechanism driving the direction of CD40-induced CD4 polarization. The CD40/CD40L costimulatory pathway both enhances and prolongs contact between CD4 T cells and B cells, inducing upregulation of CD80 and CD86 (58). It is likely that by inhibiting this pathway, tumor-promoting pro-inflammatory responses were blocked in InvRas pretreatment protocols, leading to the significant decrease in tumor number. Although our results show the importance of this pathway in regulating polarization both *in vivo* and *in vitro*, the studies in mice utilized global CD40L blockade or CD40 activation. While the results agree with our hypothesis, we cannot rule out that blockade or activation of dendritic cell and keratinocyte-based CD40 could have occurred and impacted the observed effects on tumor formation. However, the lack of differences in dendritic cell activity, and the inability for *Rag1*$^{-/-}$ mice to specifically polarize CD4 T cells or B cells in single adoptive transfers, suggests that neither keratinocytes nor dendritic cells could specifically polarize these lymphocytes, as *Rag1*$^{+/+}$ phenotypes were only observed with both CD4 T cells and B cells simultaneously present.

Our results show that the composition and functionality of the tumor immune microenvironment influence the response to therapeutic mAbs. Treatment of preexisting basal/stem cell derived tumors with anti-CD40L enhances tumor growth, whereas CD40 agonist treatment prevents new formation and growth of existing tumors. In contrast,

treatment of committed progenitor/suprabasal derived tumors with anti-CD40L inhibits tumor growth, but a CD40 agonist enhances growth of established tumors. CD40 agonist and antagonist mAbs such as dacetuzumab (Seattle Genetics) and lucatumumab (Novartis) (59) have been tested in human cancer patients with chronic lymphatic leukemia, multiple myeloma, and non-Hodgkin's lymphoma, and approximately 20% of patients with melanoma or pancreatic carcinoma treated with CP-870,893,0 (Pfiser/VLST), a CD40 agonist mAb (43), responded. CD40 agonist Chi Lob 7/4 (University of Southampton) was tested in lymphomas and advanced solid tumors, but stable disease was found to be the best response (43). With the success of immunotherapy with anti-PD1 and anti-CTLA4, as well as novel checkpoint targets in development, our results recommend specifically examining the tumor immune microenvironment prior to administration, as it may be possible to understand why some patients fail to respond, to predict the efficacy of specific immunotherapeutic drugs, to determine which single or combination of immunotherapeutics will be most effective in specific patients, and which may exacerbate conditions and allow tumor escape.

Supplementary Material

Refer to Web version on PubMed Central for supplementary material.

Acknowledgments

Financial Support: This work is supported by funds from the NIH T32 Training Grant to MAP, The Pennsylvania State University College of Agricultural Sciences to MAP and ABG, and The Elsa U. Pardee Foundation.

We thank the Huck Institutes of the Life Sciences Microscopy and Cytometry Core Facilities, the Elsa U Pardee Foundation for financial support, and Genentech for donation of CD20 mAbs. Michael Podolsky was supported through NIH T32 training grant "Animal Models of Inflammation" and The College of Agricultural Sciences, The Pennsylvania State University.

Reference List

1. Kerkar SP, Restifo NP. Cellular constituents of immune escape within the tumor microenvironment. Cancer Res. 2012; 72:3125–30. [PubMed: 22721837]
2. Eckert AW, Wickenhauser C, Salins PC, Kappler M, Bukur J, Seliger B. Clinical relevance of the tumor microenvironment and immune escape of oral squamous cell carcinoma. J Transl Med. 2016; 14:85. [PubMed: 27044404]
3. Kalathil SG, Thanavala Y. High immunosuppressive burden in cancer patients: a major hurdle for cancer immunotherapy. Cancer Immunol Immunother. 2016; 65:813–9. [PubMed: 26910314]
4. Balkwill F, Mantovani A. Inflammation and cancer: back to Virchow? Lancet. 2001; 357:539–45. [PubMed: 11229684]
5. de Visser KE, Korets LV, Coussens LM. De novo carcinogenesis promoted by chronic inflammation is B lymphocyte dependent. Cancer Cell. 2005; 7:411–23. [PubMed: 15894262]
6. Spranger S, Gajewski TF. Tumor-intrinsic oncogene pathways mediating immune avoidance. Oncoimmunology. 2016; 5:e1086862. [PubMed: 27141343]
7. Rizvi NA, Chan TA. Immunotherapy and Oncogenic Pathways: The PTEN Connection. Cancer Discov. 2016; 6:128–9. [PubMed: 26851183]
8. Varadan V, Gilmore H, Miskimen KL, Tuck D, Parsai S, Awadallah A, et al. Immune Signatures Following Single Dose Trastuzumab Predict Pathologic Response to Preoperative Trastuzumab and Chemotherapy in HER2-Positive Early Breast Cancer. Clin Cancer Res. 2016; 22:3249–59. [PubMed: 26842237]

9. Alistar A, Chou JW, Nagalla S, Black MA, D'Agostino R Jr, Miller LD. Dual roles for immune metagenes in breast cancer prognosis and therapy prediction. Genome Med. 2014; 6:80. [PubMed: 25419236]
10. Wolf D, Sopper S, Pircher A, Gastl G, Wolf AM. Treg(s) in Cancer: Friends or Foe? J Cell Physiol. 2015; 230:2598–605. [PubMed: 25913194]
11. Gounaris E, Blatner NR, Dennis K, Magnusson F, Gurish MF, Strom TB, et al. T-regulatory cells shift from a protective anti-inflammatory to a cancer-promoting proinflammatory phenotype in polyposis. Cancer Res. 2009; 69:5490–7. [PubMed: 19570783]
12. Kim HJ, Cantor H. CD4 T-cell subsets and tumor immunity: the helpful and the not-so-helpful. Cancer Immunol Res. 2014; 2:91–8. [PubMed: 24778273]
13. Fremd C, Schuetz F, Sohn C, Beckhove P, Domschke C. B cell-regulated immune responses in tumor models and cancer patients. Oncoimmunology. 2013; 2:e25443. [PubMed: 24073382]
14. Nelson BH. CD20+ B cells: the other tumor-infiltrating lymphocytes. J Immunol. 2010; 185:4977–82. [PubMed: 20962266]
15. Fujimura T, Kakizaki A, Furudate S, Kambayashi Y, Aiba S. Tumor-associated macrophages in skin: How to treat their heterogeneity and plasticity. J Dermatol Sci. 2016; 83:167–73. [PubMed: 27291068]
16. Sionov RV, Fridlender ZG, Granot Z. The Multifaceted Roles Neutrophils Play in the Tumor Microenvironment. Cancer Microenviron. 2015; 8:125–58. [PubMed: 24895166]
17. Mittal D, Gubin MM, Schreiber RD, Smyth MJ. New insights into cancer immunoediting and its three component phases--elimination, equilibrium and escape. Curr Opin Immunol. 2014; 27:16–25. [PubMed: 24531241]
18. Prieto PA, Yang JC, Sherry RM, Hughes MS, Kammula US, White DE, et al. CTLA-4 blockade with ipilimumab: long-term follow-up of 177 patients with metastatic melanoma. Clin Cancer Res. 2012; 18:2039–47. [PubMed: 22271879]
19. Khanna P, Blais N, Gaudreau PO, Corrales-Rodriguez L. Immunotherapy Comes of Age in Lung Cancer. Clin Lung Cancer. 2016; doi: 10.1016/j.cllc.2016.06.006
20. Lote H, Cafferkey C, Chau I. PD-1 and PD-L1 blockade in gastrointestinal malignancies. Cancer Treat Rev. 2015; 41:893–903. [PubMed: 26412280]
21. Topalian SL, Hodi FS, Brahmer JR, Gettinger SN, Smith DC, McDermott DF, et al. Safety, activity, and immune correlates of anti-PD-1 antibody in cancer. N Engl J Med. 2012; 366:2443–54. [PubMed: 22658127]
22. Economopoulou P, Agelaki S, Perisanidis C, Giotakis EI, Psyrri A. The promise of immunotherapy in head and neck squamous cell carcinoma. Ann Oncol. 2016; doi: 10.1093/annonc/mdw226
23. Yu GT, Bu LL, Zhao YY, Mao L, Deng WW, Wu TF, et al. CTLA4 blockade reduces immature myeloid cells in head and neck squamous cell carcinoma. Oncoimmunology. 2016; 5:e1151594. [PubMed: 27471622]
24. Ladoire S, Martin F, Ghiringhelli F. Prognostic role of FOXP3+ regulatory T cells infiltrating human carcinomas: the paradox of colorectal cancer. Cancer Immunol Immunother. 2011; 60:909–18. [PubMed: 21644034]
25. Park EJ, Lee JH, Yu GY, He G, Ali SR, Holzer RG, et al. Dietary and genetic obesity promote liver inflammation and tumorigenesis by enhancing IL-6 and TNF expression. Cell. 2010; 140:197–208. [PubMed: 20141834]
26. Lu H, Ouyang W, Huang C. Inflammation, a key event in cancer development. Mol Cancer Res. 2006; 4:221–33. [PubMed: 16603636]
27. Hsu YC, Li L, Fuchs E. Transit-amplifying cells orchestrate stem cell activity and tissue regeneration. Cell. 2014; 157:935–49. [PubMed: 24813615]
28. Blanpain C, Fuchs E. Epidermal homeostasis: a balancing act of stem cells in the skin. Nat Rev Mol Cell Biol. 2009; 10:207–17. [PubMed: 19209183]
29. Brown K, Strathdee D, Bryson S, Lambie W, Balmain A. The malignant capacity of skin tumours induced by expression of a mutant H-ras transgene depends on the cell type targeted. Curr Biol. 1998; 8:516–24. [PubMed: 9560338]

30. Lapouge G, Youssef KK, Vokaer B, Achouri Y, Michaux C, Sotiropoulou PA, et al. Identifying the cellular origin of squamous skin tumors. Proc Natl Acad Sci U S A. 2011; 108:7431–6. [PubMed: 21502497]

31. Nassar D, Latil M, Boeckx B, Lambrechts D, Blanpain C. Genomic landscape of carcinogen-induced and genetically induced mouse skin squamous cell carcinoma. Nat Med. 2015; 21:946–54. [PubMed: 26168291]

32. Darwiche N, Ryscavage A, Perez-Lorenzo R, Wright L, Bae DS, Hennings H, et al. Expression profile of skin papillomas with high cancer risk displays a unique genetic signature that clusters with squamous cell carcinomas and predicts risk for malignant conversion. Oncogene. 2007; 26:6885–95. [PubMed: 17525749]

33. Jaubert J, Patel S, Cheng J, Segre JA. Tetracycline-regulated transactivators driven by the involucrin promoter to achieve epidermal conditional gene expression. J Invest Dermatol. 2004; 123:313–8. [PubMed: 15245431]

34. Xie W, Wu X, Chow LT, Chin E, Paterson AJ, Kudlow JE. Targeted expression of activated erbB-2 to the epidermis of transgenic mice elicits striking developmental abnormalities in the epidermis and hair follicles. Cell Growth Differ. 1998; 9:313–25. [PubMed: 9563851]

35. Chin L, Tam A, Pomerantz J, Wong M, Holash J, Bardeesy N, et al. Essential role for oncogenic Ras in tumour maintenance. Nature. 1999; 400:468–72. [PubMed: 10440378]

36. Lincecum JM, Vieira FG, Wang MZ, Thompson K, De Zutter GS, Kidd J, et al. From transcriptome analysis to therapeutic anti-CD40L treatment in the SOD1 model of amyotrophic lateral sclerosis. Nat Genet. 2010; 42:392–9. [PubMed: 20348957]

37. Mohammed J, Ryscavage A, Perez-Lorenzo R, Gunderson AJ, Blazanin N, Glick AB. TGFbeta1-induced inflammation in premalignant epidermal squamous lesions requires IL-17. J Invest Dermatol. 2010; 130:2295–303. [PubMed: 20410912]

38. Gunderson AJ, Mohammed J, Horvath FJ, Podolsky MA, Anderson CR, Glick AB. CD8(+) T cells mediate RAS-induced psoriasis-like skin inflammation through IFN-gamma. J Invest Dermatol. 2013; 133:955–63. [PubMed: 23151849]

39. Mordasky Markell L, Perez-Lorenzo R, Masiuk KE, Kennett MJ, Glick AB. Use of a TGFbeta type I receptor inhibitor in mouse skin carcinogenesis reveals a dual role for TGFbeta signaling in tumor promotion and progression. Carcinogenesis. 2010; 31:2127–35. [PubMed: 20852150]

40. Wirsing AM, Rikardsen OG, Steigen SE, Uhlin-Hansen L, Hadler-Olsen E. Characterisation and prognostic value of tertiary lymphoid structures in oral squamous cell carcinoma. BMC Clin Pathol. 2014; 14:38. [PubMed: 25177210]

41. Hiraoka N, Ino Y, Yamazaki-Itoh R. Tertiary Lymphoid Organs in Cancer Tissues. Front Immunol. 2016; 7:244. [PubMed: 27446075]

42. Elgueta R, Benson MJ, de VV, Wasiuk A, Guo Y, Noelle RJ. Molecular mechanism and function of CD40/CD40L engagement in the immune system. Immunol Rev. 2009; 229:152–72. [PubMed: 19426221]

43. Vonderheide RH, Glennie MJ. Agonistic CD40 antibodies and cancer therapy. Clin Cancer Res. 2013; 19:1035–43. [PubMed: 23460534]

44. Girardi M. Immunosurveillance and immunoregulation by gammadelta T cells. J Invest Dermatol. 2006; 126:25–31. [PubMed: 16417214]

45. Denfeld RW, Hollenbaugh D, Fehrenbach A, Weiss JM, von LA, Mai B, et al. CD40 is functionally expressed on human keratinocytes. Eur J Immunol. 1996; 26:2329–34. [PubMed: 8898941]

46. Grone A. Keratinocytes and cytokines. Vet Immunol Immunopathol. 2002; 88:1–12. [PubMed: 12088639]

47. Liu S, Liu D, Li J, Zhang D, Chen Q. Regulatory T cells in oral squamous cell carcinoma. J Oral Pathol Med. 2016; doi: 10.1111/jop.12445

48. Byrne WL, Mills KH, Lederer JA, O'Sullivan GC. Targeting regulatory T cells in cancer. Cancer Res. 2011; 71:6915–20. [PubMed: 22068034]

49. Bodogai M, Lee CC, Wejksza K, Lai J, Merino M, Wersto RP, et al. Anti-CD20 antibody promotes cancer escape via enrichment of tumor-evoked regulatory B cells expressing low levels of CD20 and CD137L. Cancer Res. 2013; 73:2127–38. [PubMed: 23365136]

50. Lim KP, Chun NA, Ismail SM, Abraham MT, Yusoff MN, Zain RB, et al. CD4+CD25hiCD127low regulatory T cells are increased in oral squamous cell carcinoma patients. PLoS One. 2014; 9:e103975. [PubMed: 25153698]
51. Bron L, Jandus C, ndrejevic-Blant S, Speiser DE, Monnier P, Romero P, et al. Prognostic value of arginase-II expression and regulatory T-cell infiltration in head and neck squamous cell carcinoma. Int J Cancer. 2013; 132:E85–E93. [PubMed: 22815199]
52. Wolf GT, Chepeha DB, Bellile E, Nguyen A, Thomas D, McHugh J. Tumor infiltrating lymphocytes (TIL) and prognosis in oral cavity squamous carcinoma: a preliminary study. Oral Oncol. 2015; 51:90–5. [PubMed: 25283344]
53. Tzankov A, Meier C, Hirschmann P, Went P, Pileri SA, Dirnhofer S. Correlation of high numbers of intratumoral FOXP3+ regulatory T cells with improved survival in germinal center-like diffuse large B-cell lymphoma, follicular lymphoma and classical Hodgkin's lymphoma. Haematologica. 2008; 93:193–200. [PubMed: 18223287]
54. Amedei A, Niccolai E, Prisco D. Pancreatic cancer: role of the immune system in cancer progression and vaccine-based immunotherapy. Hum Vaccin Immunother. 2014; 10:3354–68. [PubMed: 25483688]
55. DeNardo DG, Barreto JB, Andreu P, Vasquez L, Tawfik D, Kolhatkar N, et al. CD4(+) T cells regulate pulmonary metastasis of mammary carcinomas by enhancing protumor properties of macrophages. Cancer Cell. 2009; 16:91–102. [PubMed: 19647220]
56. Waldner MJ, Neurath MF. Colitis-associated cancer: the role of T cells in tumor development. Semin Immunopathol. 2009; 31:249–56. [PubMed: 19495757]
57. Wykes M. Why do B cells produce CD40 ligand? Immunol Cell Biol. 2003; 81:328–31. [PubMed: 12848855]
58. Clark EA. Regulation of B lymphocytes by dendritic cells. J Exp Med. 1997; 185:801–3. [PubMed: 9120385]
59. Hassan SB, Sorensen JF, Olsen BN, Pedersen AE. Anti-CD40-mediated cancer immunotherapy: an update of recent and ongoing clinical trials. Immunopharmacol Immunotoxicol. 2014; 36:96–104. [PubMed: 24555495]

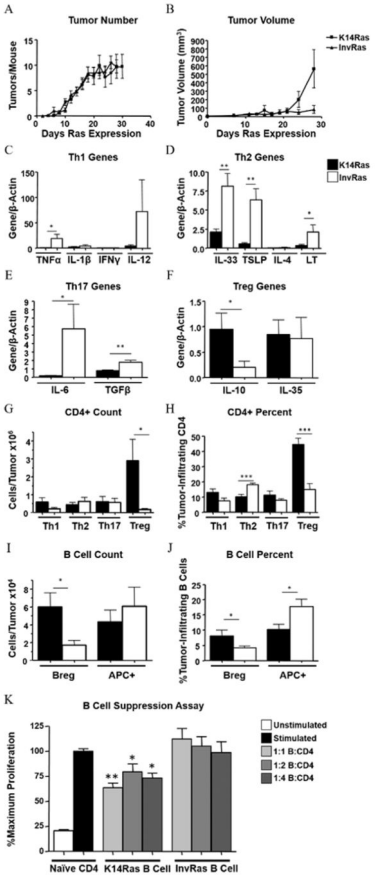

Figure 1. H-Ras^{G12V} expression in different epidermal layers determines distinct tumor phenotypes and immune responses

Tumor counts (A) and tumor volume (B) in K14Ras and InvRas mice at indicated days after Ras induction. (A: K14Ras $n = 45$, InvRas $n = 30$. B: K14Ras $n = 8$, InvRas $n = 10$). (C–F) Relative expression of specific cytokines by qPCR in whole tumor tissue associated with Th1 (C), Th2 (D), Th17 (E), and Treg (F) cells. (C: K14Ras $n = 8,16,5,15$, InvRas $n = 6,12,5,6$. D: K14Ras $n = 16,16,5,8$, InvRas $n = 12,12,5,6$. E: K14Ras $n = 8,16$, InvRas $n = 6,12$. F: K14Ras $n = 14,16$, InvRas $n = 10,10$). Samples below detection level were not used in analysis. (G–J) Analysis of tumor-infiltrating CD4 T cell counts (G), and CD4 percentages (H), tumor-infiltrating B cell counts (I), and B cell percentages (J) in K14Ras and InvRas tumors. Counts were determined using a Cellometer Auto T4 Cell Viability Counter (Nexcelom Bioscience), and quantified using FlowJo software. Counts represent $n = 12$ for CD4 T cells, $n = 11$ for B cells. Percentages represent $n \geq 15$ per group. (K) Analysis of CD4 T cell proliferation following 7 day coculture with tumor-conditioned B cells of K14Ras or InvRas mice. CFSE was analyzed by flow cytometry. Stimulated control baseline set to 100%, and significance is calculated against stimulated control group. $n = 6$ per group (2×3).

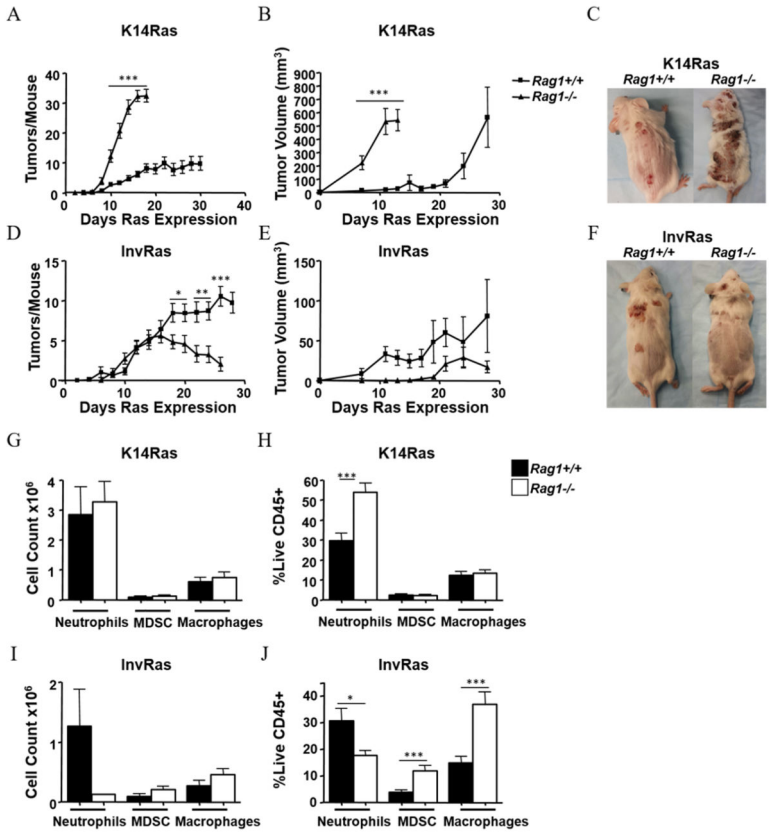

Figure 2. Lymphocytes have opposing effects on tumor development dependent on tissue compartment of H-Ras^{V12G} expression

Tumor counts (A), tumor volume (B), and representative gross phenotype at end stages (C) of K14Ras*Rag1*$^{+/+}$ and K14Ras*Rag1*$^{-/-}$ mice at indicated days after Ras induction. (A: K14Ras*Rag1*$^{+/+}$ n = 45, K14Ras*Rag1*$^{-/-}$ n = 28. B: n = 8 per group). Tumor counts (D) Tumor Volume (E) and representative gross phenotype at end stages (F) of InvRas*Rag1*$^{+/+}$ and InvRas*Rag1*$^{-/-}$ mice at indicated days after Ras induction. (D: InvRas*Rag1*$^{+/+}$ n = 30, InvRas*Rag1*$^{-/-}$ n = 27. E: InvRas*Rag1*$^{+/+}$ n = 10, InvRas*Rag1*$^{-/-}$ n = 6). (G and H) Analysis of tumor-infiltrating myeloid cell counts (G), and myeloid percentages (H) in K14Ras*Rag1*$^{+/+}$ or K14Ras*Rag1*$^{-/-}$ mice. (G: K14Ras*Rag1*$^{+/+}$ n = 12, K14Ras*Rag1*$^{-/-}$ n = 12. H: K14Ras*Rag1*$^{+/+}$ n = 30, K14Ras*Rag1*$^{-/-}$ n = 15). (I and J) Analysis of tumor-infiltrating myeloid cell counts (I), and myeloid percentages (J) in InvRas*Rag1*$^{+/+}$ or InvRas*Rag1*$^{-/-}$ mice. (I: InvRas*Rag1*$^{+/+}$ n = 12, InvRas*Rag1*$^{-/-}$ n = 4. J: InvRas*Rag1*$^{+/+}$ n = 21, InvRas*Rag1*$^{-/-}$ n = 18). Counts were determined using a Cellometer Auto T4 Cell Viability Counter (Nexcelom Bioscience), and quantified using FlowJo software.

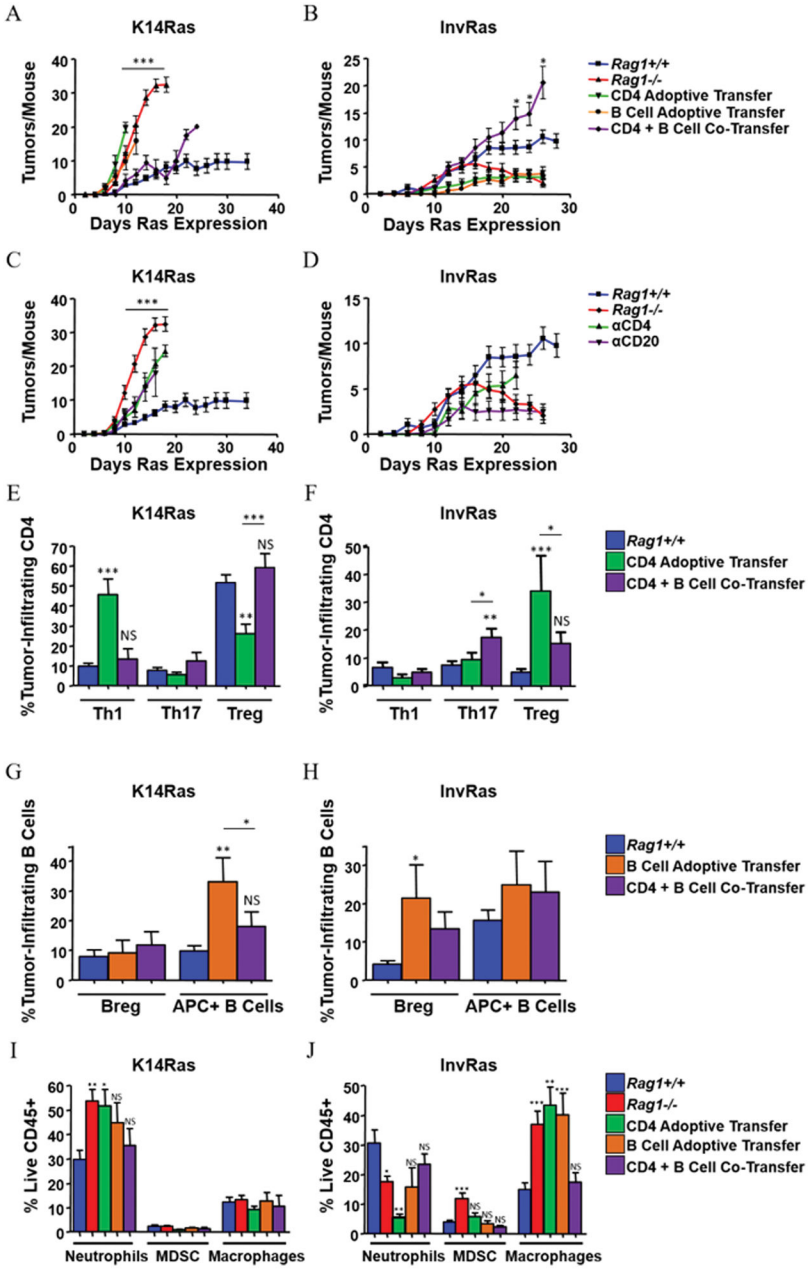

Figure 3. CD4 T Cells and B Cells cooperate in K14Ras and InvRas mice to produce protective and tumor-promoting immune responses, respectively

(A and B) Tumor counts in adoptively transferred K14Ras*Rag1*$^{-/-}$ (A) and InvRas*Rag1*$^{-/-}$ (B) mice at indicated days after Ras induction. K14Ras*Rag1*$^{+/+}$, K14Ras*Rag1*$^{-/-}$, InvRas*Rag1*$^{+/+}$, and InvRas*Rag1*$^{-/-}$ mice from previous figures included as reference. (A: n = 45, 28, 12, 13, and 18. B: n = 30, 27, 12, 12, and 12). (C and D) Tumor counts in CD4 and CD20-depleted mice of K14Ras (C) and InvRas (D) mice at indicated days after Ras induction. K14Ras*Rag1*$^{+/+}$, K14Ras*Rag1*$^{-/-}$, InvRas*Rag1*$^{+/+}$, and InvRas*Rag1*$^{-/-}$ mice from previous figures included as reference. (C: n = 45, 28, 12, and 13. D: n = 35, 27, 12, and 18). (E and F) Analysis of tumor-infiltrating CD4 percentages in K14Ras (E) and InvRas (F)

adoptive transfer experiments into *Rag1*$^{-/-}$ mice. (E: $n \geq 11$ for all groups. F: $n \geq 7$ for all groups). (G and H) Analysis of tumor-infiltrating B cell percentages in K14Ras (G) and InvRas (H) adoptive transfer experiments into *Rag1*$^{-/-}$ mice. (G: $n \geq 6$ for all groups. H: $n \geq 6$ for all groups). (I and J) Analysis of tumor-infiltrating myeloid percentages in K14Ras (I) and InvRas (J) adoptive transfer experiments into *Rag1*$^{-/-}$ mice. (I: $n \geq 11$ for all groups. J: $n \geq 6$ for all groups). Unless otherwise indicated, significance was calculated compared to *Rag1*$^{+/+}$ mice.

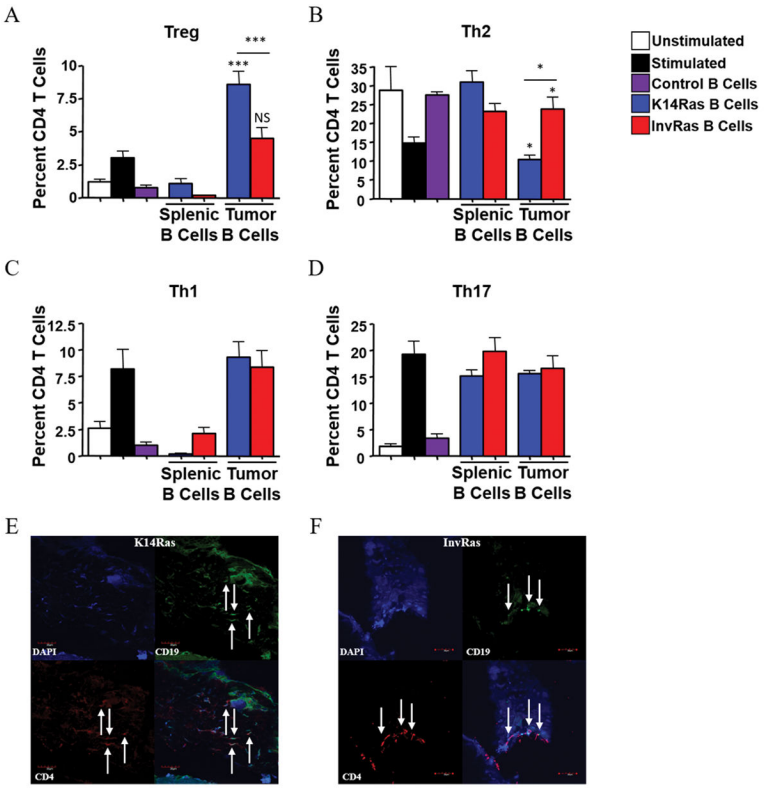

Figure 4. Direct contact between CD4 T cells and tumor-conditioned B cells is essential for CD4 T cell polarization and phenotype

(A–D) Analysis of CD4 percentages following 7-day coculture with control splenic B cells from healthy mice, splenic B cells from tumor-bearing K14Ras or InvRas mice, or B cells from tumor tissue of K14Ras or InvRas mice, examining Treg (A), Th2 (B), Th1 (C), and Th17 (D) cells. Unstimulated and stimulated controls $n = 18$ (6 biological replicates × 3 technical replicates), Control B cells $n = 9$ (3 biological replicates × 3 technical replicates), K14Ras splenic B cells $n = 6$ (3 biological replicates × 2 technical replicates), InvRas splenic B cells $n = 9$ (3 biological replicates × 3 technical replicates), Tumor B cells minimum $n = 24$ (8 biological replicates × 3 technical replicates) maximum $n = 36$ (12 biological replicates × 3 technical replicates). Unless otherwise indicated, significance was calculated compared to stimulated control group. (E and F) Immunofluorescence examination of CD4 (Red), CD19 (Green), DAPI (Blue), and composite of representative K14Ras (E) and InvRas (F) tumors. Arrows indicate CD4 and B Cells in direct contact. Magnification: 10x.

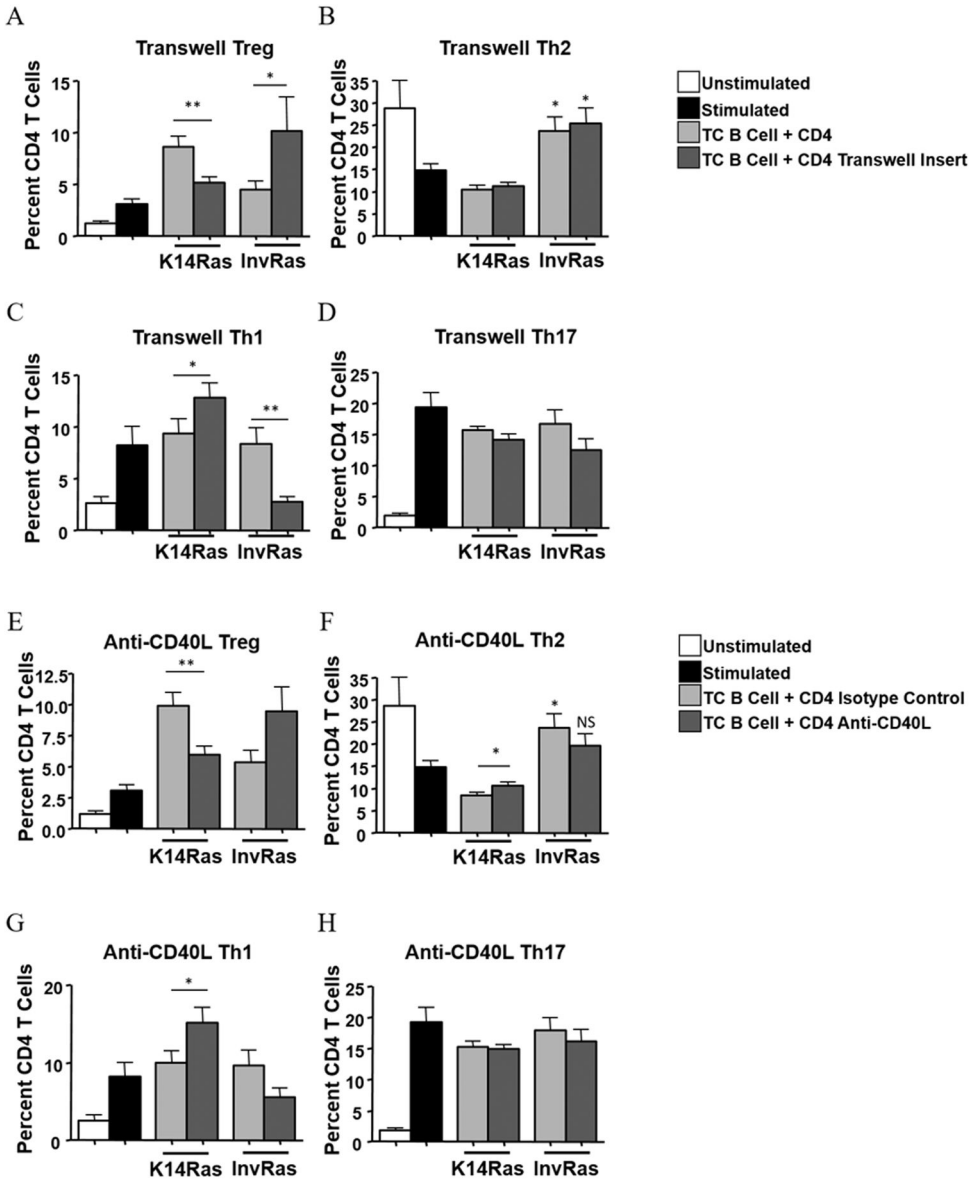

Figure 5. CD4 T-cell polarization by tumor-conditioned B cells is reliant on direct cell contact and CD40 signaling

(A–D) Analysis of CD4 percentages following 7-day coculture with B Cells from tumor tissue of K14Ras or InvRas mice with or without transwell inserts examining Treg (A), Th2 (B), Th1 (C), and Th17 (D). Unstimulated and Stimulated controls $n = 18$ (6 biological replicates × 3 technical replicates) and Tumor B cells minimum $n = 24$ (8 biological replicates × 3 technical replicates) maximum $n = 36$ (12 biological replicates × 3 technical replicates) from Fig. 4 included as reference. Transwell insert groups minimum $n = 24$ (8 biological replicates × 3 technical replicates), maximum $n = 36$ (12 biological replicates × 3 technical replicates). (E–H) Analysis of CD4 percentages following 7-day coculture with B Cells from tumor tissue of K14Ras or InvRas mice with or without Anti-CD40L examining Treg (E), Th2 (F), Th1 (G), and Th17 (H). Unstimulated and Stimulated controls $n = 18$ (6 biological replicates × 3 technical replicates) from Fig. 4 included as reference. Isotype

control and Anti-CD40L groups minimum $n = 24$ (8 biological replicates × 3 technical replicates), maximum $n = 36$ (12 biological replicates × 3 technical replicates). Unless otherwise indicated, significance was calculated compared to stimulated control group.

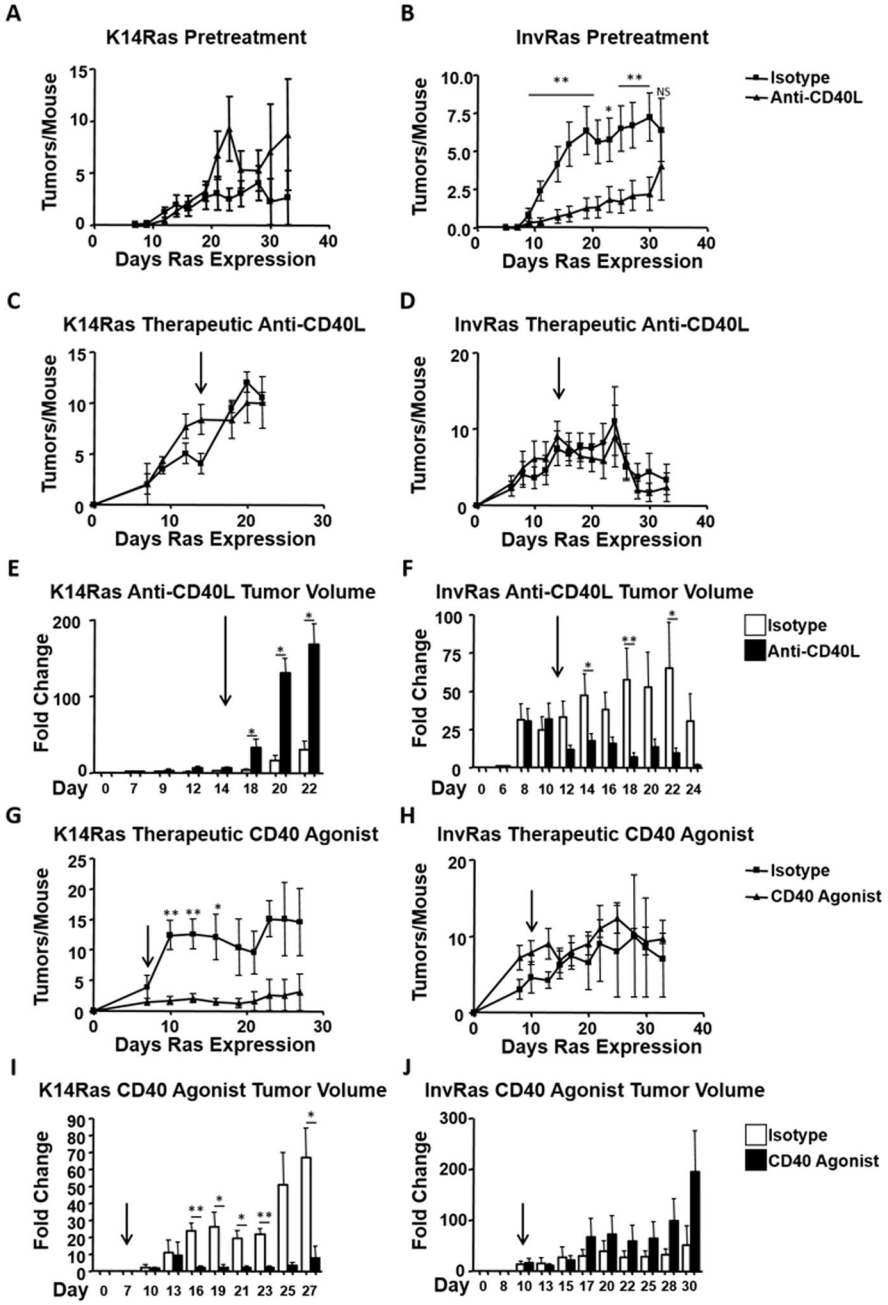

Figure 6. Continuous stimulation through CD40/CD40L is required for a sustained anti-tumor immune response

(A and B) Tumor counts in isotype control and anti-CD40L pretreatment injected K14Ras (A) and InvRas (B) mice at indicated days after Ras induction. (A: isotype $n = 17$, anti-CD40L $n = 18$, B: isotype $n = 15$, anti-CD40L $n = 16$). (C and D) Tumor counts in isotype control and anti-CD40L therapeutic protocol injected K14Ras (C) and InvRas (D) mice at indicated days after Ras induction. Arrows indicate day of first treatment. (C: isotype $n = 8$, anti-CD40L $n = 7$, D: isotype $n = 7$, anti-CD40L $n = 8$). (E and F) Average fold increase in tumor volume from starting measurements at indicated days of therapeutically injected

K14Ras (E) and InvRas (F) mice. Arrows indicate day of first treatment. (G and H) Tumor counts in Isotype control and CD40 Agonist injected K14Ras (G) and InvRas (H) mice at indicated days after Ras induction. Arrows indicate day of first treatment. (G: isotype $n = 6$, anti-CD40L $n = 5$, H: isotype $n = 5$, anti-CD40L $n = 6$). Average fold increase in tumor volume from starting measurements in CD40 Agonist protocols at indicated days of K14Ras (I) and InvRas (J) mice. Arrows indicate day of first treatment.